Numerical simulation investigations of the effects of noise and detection error in an adaptive optics system

Hai-Xing Yan*, She Chen, Shu-Shan Li
Institute of Mechanics, Chinese Academy of Sciences, Beijing 100080, China

ABSTRACT

In an adaptive optics (AO) system, noise and detection error can produce errors in the slope measurement of a Hartmann-Shack (HS) wavefront sensor and have further effects on the performance of the AO System. The noise in an AO system can be divided into the readout noise and the photon noise. The detection error in an AO system results from the discrete sampling by using number-limited CCD pixels in the HS sensor and the deadspace between the CCD pixels. A theoretical model for numerically simulating the effects of noise and detection error is presented and a corresponding computer program has been compiled, which is combined with our existing program of numerical simulation of the laser propagation in a turbulent media and an AO system in a stationary state. Taking the long-exposure Strehl ratio and the percentage relative error of the centroid slopes for each subaperture as two evaluation parameters, numerical simulation investigations of the effects of detection error (including the limited sampling density and the deadspace), readout noise and photon noise on a practical AO system have been carried out. Statistics method and formulation method are used to evaluate the effects of readout noise and photon noise in the numerical simulation. It is shown that there is no significant difference between results by using these two methods when the signal to noise ratio (SNR) is larger. However, as SNR gets smaller, the formulation method becomes less accurate than the statistics method. The numerical results are very useful for the design of a practical AO system.

Keywords: adaptive optics system, numerical simulation, noise, detection error, Hartmann-Shack wavefront sensor, signal to noise ratio (SNR)

1. INTRODUCTION

It is well known that an adaptive optics (AO) system can make real -time wavefront detection and correction to significantly improve the image quality of optical wave after propagating in the turbulent atmosphere. Therefore, it has been widely applied in improving the astronomical observation of ground-based telescope and the laser beam propagation.[1,2]

It is also well known that modeling and numerical simulation can provide important assistances to the design, examination, investigation and application of a complex integrated system like an AO system. Modeling and numerical simulation can provide an accurate evaluation for different schemes of a new AO system in progress to make a theoretical design. For an existing AO system, a numerical simulation can do the numerical experiments with much less expense and much more convenience. Furthermore, it is possible to do an insight investigation by means of a numerical simulation even on an impractical or extreme condition for an existing AO system. Among numerous publications on the AO system, a few relate to modeling and numerical simulation of an AO system.[3-5] However, they are generally descriptive or introductive. We have

* Correspondence: Email: hxyan@imech.ac.cn; Phone: (86) 10 62554123; Fax: (86) 10 62561284

Adaptive Optics Systems and Technology II, Robert K. Tyson, Domenico Bonaccini, Michael C. Roggemann, Editors, Proceedings of SPIE Vol. 4494 (2002)

been pursuing modeling and numerical simulation of an AO system in the past decade. Our most recent English publication was about numerical simulation of laser propagation in the atmosphere and an adaptive optics system in stationary state.[6]

There are three important factors to affect the performances of an AO system. The first of them is the limited spatial bandwidth resulted from the limited numbers of the sub-apertures for wavefront detection and the actuators in the deformable mirror for wavefront correction. [6] The second is effects of noise and detection error. The third is the limited temporal bandwidth resulted from the limited response speed for wavefront detection, reconstruction and correction. This paper will focus on the effects of noise and detection error in an AO system and a companion paper[7] will focus on the dynamic control process and frequency response characteristics in an AO system. Thus, a comprehensive modeling and numerical simulation of an AO system is completed in this way.

The effects of noise and detection error on performances of an AO system are in terms of the measurement error of optical centroid in the widely-used Hartmann-Shack (HS) wavefront sensor in an AO system. The effects of noise and detection error in an AO system can be divided into three parts[8,9]: (i) detection error from the number-limited discrete sampling (herein, there are two kinds of limited numbers, first, number of subapertures in a HS wavefront sensor is limited, second, number of CCD pixels for detecting the optical centroid of each subaperture is limited, the first concern is discussed in another paper[6] and only the second one is included in this paper); (ii) readout noise; and (iii) photon noise.

In this paper, these three parts are theoretically analyzed and an analytical formula for effects of readout noise and photon noise on measurement in a HS sensor is derived. Based on the theoretical analysis, a theoretical model for numerically simulating the effects of noise and detection error in an AO system is presented. A corresponding computer program is compiled and combined with our existing computation program of numerical simulation of laser propagation in the atmosphere and an AO system[6]. A series of computational results are obtained to do numerical simulation investigations. These results are very useful for the design and application of a practical AO system.

2. THEORETICAL ANALYSIS

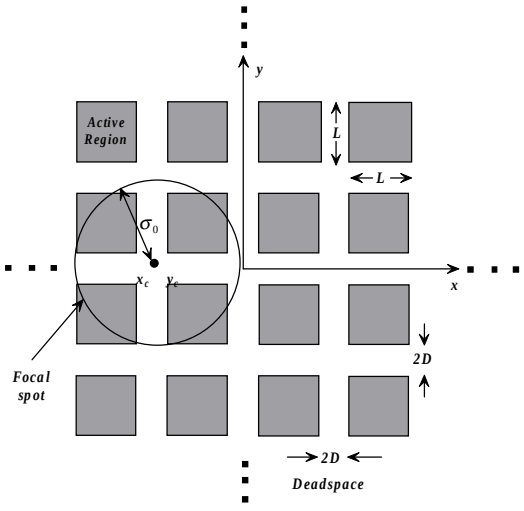

Fig. 1 Diagram of detecting the optical centroid by means of a discrete CCD array.

There are two reasons to create detection error in a HS wavefront sensor. The first of them is that number-limited discrete CCD pixels are used to measure the optical centroid for each subaperture. The second is there is a deadspace between two adjacent CCD pixels (see Fig. 1).[8-10] It is difficult for the detection error to derive an accurate analytical formula to describe its effect on determining centroid in a HS wavefront sensor. However, it is easy and convenient in a numerical simulation to numerically calculate focusing and centroiding of turbulence-distorted optical wave for each subaperture according to the realistic distribution of CCD pixels for that subaperture. In more details, the wave field of the beam that radiates from a beacon propagates through a turbulent atmosphere and strikes the HS sensor. The wave

field is divided into several subapertures and the wave field of a subaperture propagates to reach the focal plane (CCD pixels) of the HS sensor. The centroid position for each subaperture can be calculated by using the detected photon events in all related CCD pixels. Furthermore, the average slopes of the subaperture in x and y directions can be determined. It is completely natural to include the effects of the detection error on a HS wavefront sensor in a numerical si mulation.

The effects of the readout noise and photon noise on a HS sensor is in terms of affecting the photon events detected by each CCD pixel.[8,10] A centroid position of a image spot detected by a group of CCD pixels is given by the following expressions for x_c and y_c:

$$x_c = \sum_{i,j}^{L,M} x_i n_{ij} \Big/ \sum_{i,j}^{L,M} n_{ij} \quad \text{and} \quad y_c = \sum_{i,j}^{L,M} y_j n_{ij} \Big/ \sum_{i,j}^{L,M} n_{ij} , \tag{1}$$

where x_i, y_j, and n_{ij} are the coordinates and photon events associated with the pixel in column i and row j of the CCD array, respectively, L and M are the pixel numbers in x and y directions for each subaperture, respectively, and they may be different. Because the expressions for x_c and y_c are quite similar, it is enough to focus only on the expression for x_c.

Using an expression of $x_c = u/v$, where

$$u = \sum_{i,j}^{L,M} x_i n_{ij} \quad \text{and} \quad v = \sum_{i,j}^{L,M} n_{ij} , \tag{2}$$

according to the generalized law of error propagation, the error variance s_x^2 in x_c can be derived as

$$s_x^2 = \frac{s_u^2}{v^2} + \frac{u^2 s_v^2}{v^4} - \frac{2u s_{uv}}{v^3} , \tag{3}$$

where s_u^2 and s_v^2 are the variance in the measurements of u and v, respectively, and s_{uv} is the covariance of these quantities. The following equations can be derived:

$$s_u^2 = \sum_{i,j}^{L,M} s_{ij}^2 x_i^2 + \sum_{ij \neq kl}^{L,M} s_{ijkl} x_i x_k , \tag{4}$$

$$s_v^2 = \sum_{i,j}^{L,M} s_{ij}^2 + \sum_{ij \neq kl}^{L,M} s_{ijkl} , \tag{5}$$

$$s_{uv} = \sum_{i,j}^{L,M} s_{ij}^2 x_i + \sum_{ij \neq kl}^{L,M} s_{ijkl} x_i , \tag{6}$$

where s_{ij}^2 is the variance of n_{ij}, and s_{ijkl} is the covariance of the photon events between the ijth pixel and the klth pixel. On a practical condition, it can be justified that to ignore the covariance between pixels is a very good approximation.

When the readout noise and the photon noise are included, we have $s_{ij}^2 = \sigma_p^2 + \sigma_r^2$, where σ_r^2 is the variance of the readout noise and σ_p^2 is the variance of the photon noise. The photon noise obeys a Poisson statistics and the variance in a

Poisson statistics is equal to the average. That is, $\sigma_p^2 = n_{ij}$ and

$$s_{ij}^2 = n_{ij} + \sigma_r^2 . \tag{7}$$

Eqs. (4)-(7) are substituted into Eq. (3) to find

$$S_x^2 = (\sigma_x^2 + \sigma_r^2 f) / \sum_{i,j}^{L,M} n_{ij} , \tag{8}$$

where σ_x is the width of the spot given by

$$\sigma_x = (\overline{x^2} + \bar{x}^2)^{1/2} , \tag{9}$$

and

$$f = (\sum_{i,j}^{L,M} x_i^2 + N\bar{x}^2 - 2\bar{x}\sum_{i,j}^{L,M} x_i) / \sum_{i,j}^{L,M} n_{ij} , \tag{10}$$

$$\bar{x} = \sum_{i,j}^{L,M} x_i n_{ij} / \sum_{i,j}^{L,M} n_{ij} , \tag{11}$$

$$\overline{x^2} = \sum_{i,j}^{L,M} x_i^2 n_{ij} / \sum_{i,j}^{L,M} n_{ij} . \tag{12}$$

Eq. (8) is the analytical expression of effects of the readout noise and the photon noise on the x_c for a subaperture. The expression for the error in y_c is identical except that y_j will substitute for x_i.

3. NUMERICAL COMPUTATION

When numerically calculating effects of the readout noise and the photon noise on an AO system, we utilize two methods. The first of them is called as formulation method. In detail, Eq. (8) is used to calculate the variance s_x^2 in x_c for a subaperture in the formulation method, then, a random process which variance is equal to s_x^2 is assumed to obey the Gauss statistics to randomly produce the change (error) of x_c due to the effects of the readout noise and photon noise for that subaperture in a random process realization. This change (error) of x_c is then added to the x_c without any noise to obtain the centroid position in x direction with noise effects. The centroid position in y direction with noise effects can be calculated in the same way. It is shown in the later computational results that the analytical formula is a very good approximation on the condition of higher signal-to-noise ratio (SNR); but, when SNR is smaller, the results of formulation method differ a little from the practical results. It may be because some approximations are included in deriving Eq. (8) and a Gauss statistics is assumed for the random process producing error in the centroid position. The analytical formula Eq. (8) may be useful in system analyses and error estimation. Even in a numerical simulation the formulation method is a good alternative on the condition of higher SNR and/or hoping to save computing time.

The second method is called as statistics method. In this method, the effects of the readout noise and photon noise on an AO system are directly computed in a numerical simulation. In detail, it is considered that the photon events n_{ij} in Eq. (1) must add a random increment Δn_{ij} due to the photon noise having variance n_{ij}, which obeys a Poisson statistics, and due

to the readout noise having variance σ_r^2, which is assumed to obey a Gauss statistics. The random increment Δn_{ij} is added to n_{ij} without any noise to be substituted into Eq. (1) to directly obtain the centroid position with noise effects. In this way the effects of the readout noise and photon noise on an AO system are accurately and naturally included in the calculated slopes.

Next, the numerical simulation of effects of the readout noise and the photon noise on an AO system is combined with our existing numerical simulation of laser beam propagation in the turbulent atmosphere and an AO system in stationary state[6] to do numerical simulation investigations of the effects of readout noise and photon noise on the performances of an AO system. The main idea of the numerical simulation is as follows. An optical wave from a beacon propagates through a turbulent atmosphere to reach a HS sensor with a distorted wavefront. The incident optical wave is divided into several subapertures according to the practical pattern in the HS sensor. The optical wave field of each subaperture is focused at discrete CCD pixels of a certain number and the centroid displacements relative to the centroid without wavefront distortion are obtained. The distorted wavefront is reconstructed by a reconstructor from the measured average slopes of all subapertures. In this paper the direct-gradient reconstruction algorithm[6,11] is utilized for this purpose. The reconstructed wavefront is corrected by a deformable mirror and a 2-axis fast steering mirror in the AO system. Finally, a phase-compensated beam from the outgoing laser propagates in the same, but translated (because of the time delay in the AO system and the lateral wind and/or lateral movements of target and outgoing laser) turbulent medium again to reach the target. A number of patterns at target corresponding to different turbulence realizations are accumulated to obtain a long-exposure pattern. In this paper, a number of 100 is used. A centroid is determined from the long-exposure pattern. The Strehl ratio *S* is defined as the ratio of the optical energies within a circle around the centroid with a radius of the first dark ring in the Airy pattern after propagations through the turbulent medium and through a vacuum. *S* in this paper is *STRCC* in Ref. 6 and is used to evaluate the phase compensation effectiveness of an AO system. The whole process is similar to the experimental observation.

Another parameter is presented to evaluate effects of the noises and the detection error on an AO system. It is defined as a relative error of the centroid displacement (corresponding to the average slope) x_{ckl}' and y_{ckl}' of *l*th subaperture in the *k*th sampling with effects of the noises and the detection error divide by the centroid displacement x_{ckl} and y_{ckl} without effects of the noises and the detection error according to the expression:

$$E_r(\%) = \left(\frac{100}{L}\right) \bullet \left(\sum_{l=1}^{L} \left(\frac{1}{K} \bullet \sum_{k=1}^{K} \left(\frac{1}{2} \bullet \left(\frac{(x'_{ckl} - x_{ckl})^2}{x_{ckl}^{\ 2}} + \frac{(y'_{ckl} - y_{ckl})^2}{y_{ckl}^{\ 2}} \right) \right) \right) \right), \qquad (13)$$

where *K* is the total subaperture number in the HS wavefront sensor and *L* is the total sampling number. The parameter $E_r(\%)$ is called as percentage relative error.

In the next section, taking the percentage relative error $E_r(\%)$ defined in Eq. (13) and the long-exposure Strehl ratio *S* as evaluation parameters, numerical simulation results of effects of the noises and the detection error on an AO system are presented. Apparently, $E_r(\%)$ can directly express the effect of a factor on the measurement accuracy of centroid displacement. However, it is difficult to evaluate the effect of that factor on the performance of an AO system by only using $E_r(\%)$. The long-exposure Strehl ratio *S* must also be used because it can express the final effectiveness of phase compensation in an AO system and it is the parameter which is mostly concerned by experimenters and is most widely used in the experimental observation. Although there are many factors to affect *S* in quite complicated ways, but, most results

presented in the next section relate to the effect of a single factor. Therefore, it is possible to evaluate the effect of a factor on the phase compensation effectiveness by using the effect of that factor on *S*. Furthermore, it is shown from the results presented in the next section that the percentage relative error is often much more sensitive than the Strehl ratio. In some cases, a factor does not have significant effect on *S*, but $E_r(\%)$ shows a significant change. This is why it is better to combine these two parameters to evaluate effects of the noises and the detection error of a single factor or several factors on an AO system.

4. RESULTS AND DISCUSSIONS

In this section, first, the effect of computational grid density on the computational results and the effect of the size of focal spot in a subaperture on the computational results are shown and discussed. Because effects of different factors in the noises and the detection error on an AO system have some cross-linking, for easily understanding, results and discussions are divided into four portions: effect of the number-limited discrete sampling error; effect of the readout noise; effect of the photon noise; and comprehensive effect of these three factors. Finally, the statistics method and the formulation method in computing effects of the readout noise and the photon noise are compared.

4.1 Effect of the grid density on computational results

In a numerical computation, a proper grid density must be chosen. If the grid density is too large, the computing time will be unnecessarily long. But, if the grid density is too small, the computational results will not be accurate enough to describe the effects. In Fig. 2, computational results of two grid densities are shown. When grid number of 256×256 is used in computing the laser propagation, the corresponding computation grid number for each subaperture is 64×64. When grid number of 512×512 is used in computing the laser propagation, the corresponding computation grid number for each subaperture is 128×128.

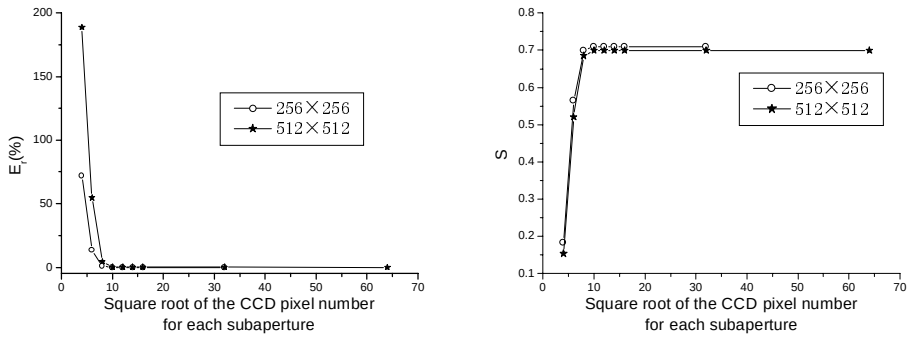

Fig. 2 Effects of computation grid density on the computational results of numerical simulation.

Computational conditions: horizontal propagation of a laser beam within distance of one kilometer, focused beam, wavelength of both beacon beam and main laser beam is 0.6328 micrometer, 10 phase screens, $C_n^2 = 10^{-14.5} m^{-2/3}$, atmospheric coherence length $r_0 = 9.63$ *cm*; adaptive optics system of 61 elements (with 48 subapertures), there is no deadspace between the CCD pixels, without the readout noise and the photon noise, lateral wind speed $v = 3$ *m/s*, the delay time $t = 5$ *ms*, 100 turbulence realizations.

It can be seen in Fig. 2 that the computational results of two grid numbers are comparable. Especially, when the CCD pixel number for each subaperture is larger, the difference between two curves is negligible. Even like this, in order to be more accurate a grid number of 512×512 is used in computing the laser propagation in this paper.

4.2 Effect of spot radius for each subaperture on the computational results

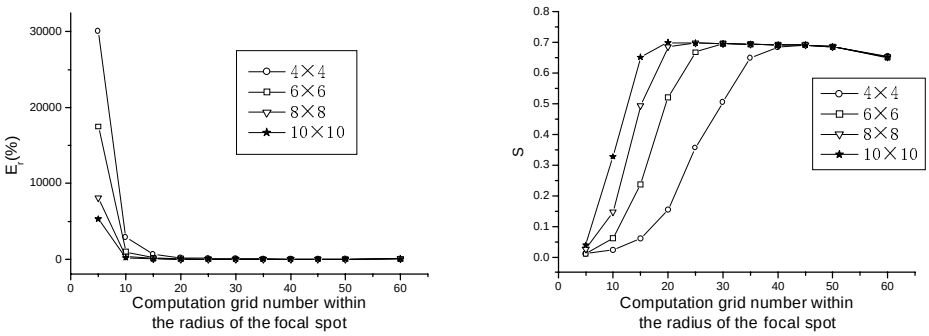

Fig. 3 Effects of the radius of focal spot for each subaperture on the computational results of numerical simulation.

Computational conditions: same as those in Fig. 2.

In the numerical computation, it is found that under the condition of a certain sampling density which is defined as the CCD pixel number for each subaperture, when the spot radius on the focal plane (i.e. on the CCD target plane) of each subaperture is different, i.e. when relative comparison of the spot size to the CCD pixel size is different, the wavefront detection and phase compensation in an AO system are influenced. Computational results for several interesting sampling densities are shown in Fig. 3. The CCD pixel number for each subaperture is shown within the rectangle in Fig. 3 and the computation grid number for each subaperture is 128×128. Generally, the computation grid number is larger than the CCD pixel number, i.e. a number of grids may be included in a CCD pixel. It is shown in Fig. 3 that there is an optimum spot radius for each sampling density. On the optimum condition the phase compensation effectiveness is optimum. This optimum spot radius can be expressed by the computation grid number within the spot radius. It is noted that the effects of the spot radius in the numerical simulation depend on the sampling density and the optimum spot radius is different for a different sampling density. The following computational results are obtained on such optimum condition for different sampling density.

4.3 Error of number-limited discrete sampling

There are two factors in this aspect: the sampling density expressed by the corresponding CCD pixel number for each subaperture and size of the deadspace between two adjacent CCD pixels.

4.3.1 Sampling density

It can be seen from Fig. 4 that when the sampling density is larger than a certain value the computational results are substantially same. This certain value can be thought as the necessary pixel number for the AO system on the corresponding condition. Although a further increase of the sampling density can produce a small amount of performance improvement, this increase will result in a corresponding increase of total CCD pixel number to create a decrease of sampling rate and thus a longer time delay. These negative effects on the performance of an AO system are much larger than the small amount of performance improvement, as shown hereinafter. Therefore, it is quite important to determine this certain value of necessary CCD pixel number. This value has a direct relationship to the practical arrangements in an AO system.

4.3.2 Deadspace between two adjacent CCD pixels

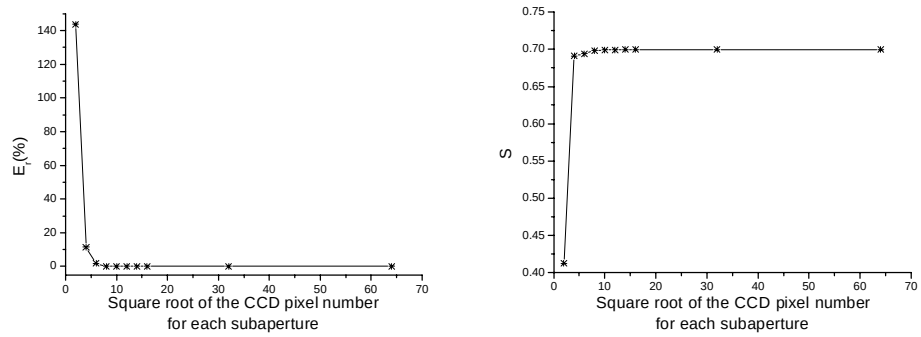

Fig. 4 Effects of the CCD pixel number for each subaperture on the computational results of numerical simulation.
Computational conditions: same as those in Fig. 2.

It can be seen from Fig. 5 that when the sampling density expressed by the CCD pixel number for each subaperture is different, the effect of the deadspace size on an AO system is also different. The deadspace size is expressed by proportion of the deadspace, which is defined as ratio of deadspace length and total length of each pixel (in Fig. 1 this deadspace proportion is *2D/(2D+L)*). As the sampling density decreases, the effect of deadspace size increases. In the case of larger pixels number (8×8), even a deadspace proportion of 0.50 does not have serious effect on the performance of an AO system. Of course, there is another factor which must be considered, that is, as deadspace size increases the corresponding effective detection area of CCD device decreases and thus detectable photon events decrease to create larger noise. In the case of smaller pixel number (4×4), the effect of deadspace is more significant. In practice, the deadspace proportion is generally smaller than 0.1. Our simulation computation shows that on this condition the effect of deadspace is not important.

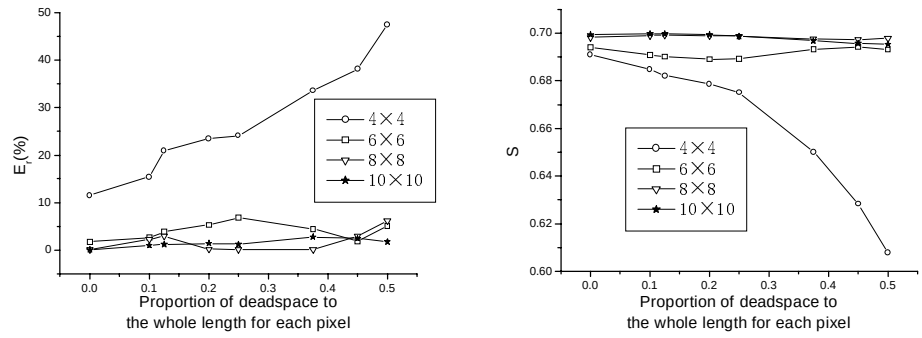

Fig. 5 Effects of the deadspace between two CCD pixels on the computational results of numerical simulation.
Computational conditions: same as those in Fig. 2 besides those indicated in this figure.

Besides the two factors mentioned above, there are some other factors in a practical AO system to affect the wavefront detection and further to influence the performance of the AO system, such as nonuniformity in size and/or sensitivity of CCD pixel, failure of individual pixel, nonuniformity in deadspace size, etc. By using a numerical simulation of this paper, all these factors can be conveniently calculated and investigated in a quantitative way.

4.4 Effect of the readout noise

It can be seen from Fig. 6 that when the SNR (SNR= n_{ij} / σ_r for the readout noise) is larger than a certain value, both Strehl ratio *S* and the percentage relative error $E_r(\%)$ approach to a stable value. In the computation a typical photon event number is chosen. However, in practice this number is related to the SNR.

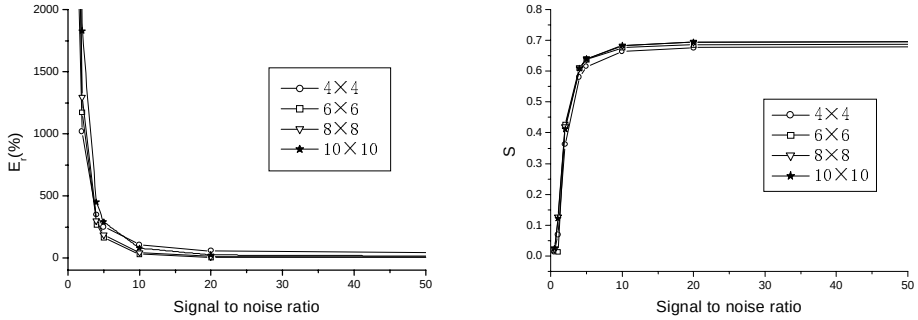

Fig. 6 Effects of the readout noise on the computational results of numerical simulation.
Computational conditions: without the photon noise, proportion of the deadspace is 0.125, counts of photon events for each CCD pixel are 10, others are same as those in Fig. 2 besides tho se indicated in this figure.

4.5 Effect of the photon noise

Results shown in Fig. 7 are quite similar to those in Fig. 6. Again, SNR (SNR= $n_{ij} / \sqrt{n_{ij}}$ for the photon noise) is the determining parameter. When SNR is larger than a certain value, both Strehl ratio *S* and the percentage relative error $E_r(\%)$ approach to a stable value. Note that because the photon noise only relates to the photon events, in order to decrease the effect of photon noise the photon event counts must be larger than a certain value.

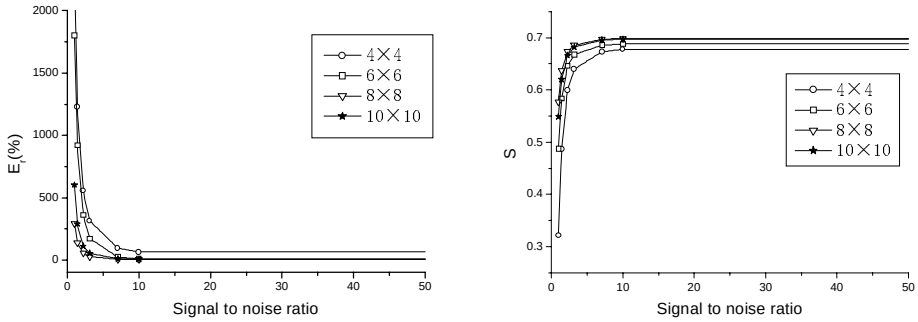

Fig. 7 Effects of the photon noise on the computational results of numerical simulation.
Computational conditions: without the readout noise, proportion of the deadspace is 0.125, others are same as those in Fig. 2 besides those indicated in this figure.

4.6 Comprehensive effect of three factors of noises and detection error

Hereinabove the respective effects of the number-limited discrete sampling, the readout noise and the photon noise are discussed. However, in fact these three factors exist in an AO system at the same time and the performance of the AO system is practically influenced by a comprehensive effect of these factors. It is shown above that effect of the deadspace between two adjacent CCD pixels on the performance of an AO system is negligible in practice. Thus, there are only three

changeable factors for improving the performance of an AO system: (1) SNR (when readout noise and photon noise exist at the same time, SNR= $n_{ij} / \sqrt{n_{ij} + \sigma_r^2}$); (2) the sampling density, i.e. the CCD pixel number for each subaperture; (3) the corresponding change of time delay due to a change of CCD pixel number for each subaperture.

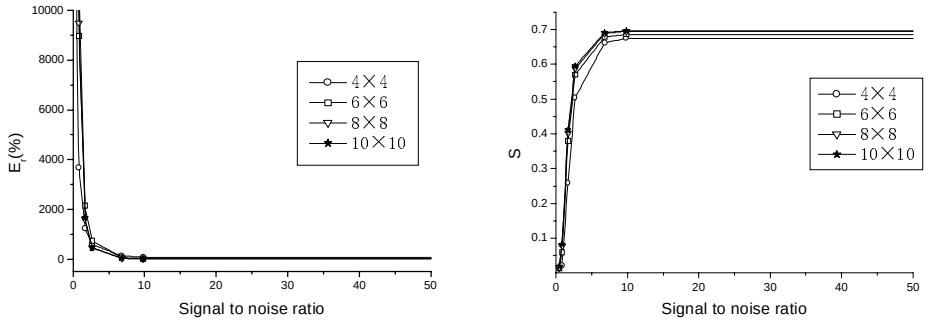

Fig. 8 Effects of the photon noise and the readout noise on the computational results of numerical simulation .
Computational conditions: proportion of the deadspace is 0.125, $\sigma_r = 2$, others are same as those in Fig. 2 besides those indicated in this figure.

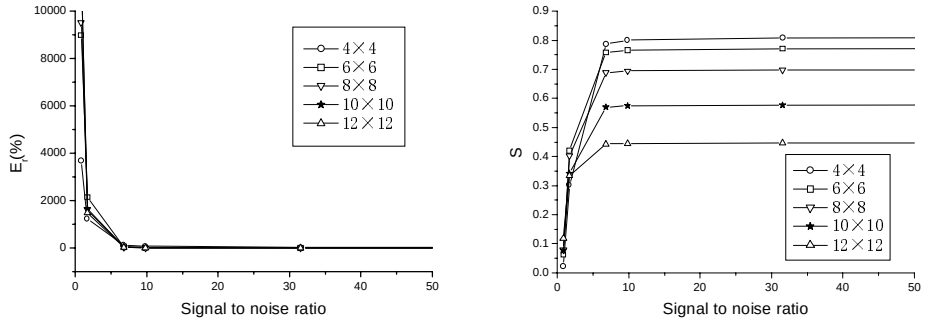

Fig. 9-1 Comprehensive effect of several factors on the computational results o f numerical simulation ($\sigma_r = 2$).

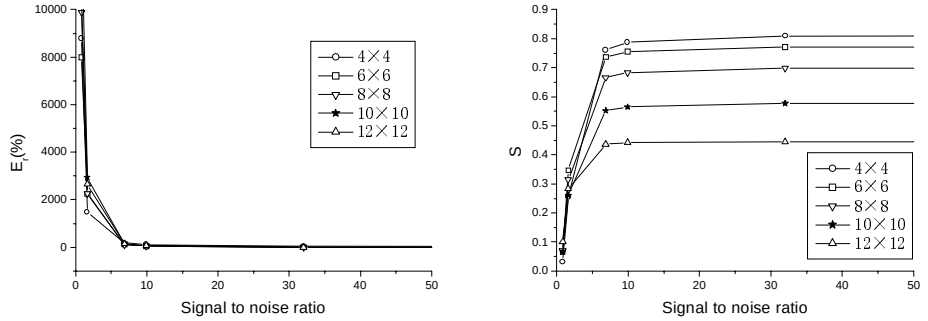

Fig. 9-2 Comprehensive effect of several factors on the computational results of numerical simulation ($\sigma_r = 30$).
Computational conditions: proportion of the deadspace is 0.125, the delay time when the pixel number for each subaperture is 4×4 is 1.25 *ms*, the delay time for the pixel number of 6×6 is 2.81 *ms*, the delay time for the pixel number of 8×8 is 5.00 *ms*, the delay time for the pixel number of 10×10 is 7.81 *ms*, the delay time for the pixel number of 12×12 is 11.25 *ms*, others are same as those in Fig. 2 besides those indicated in this figure.

The effect of SNR on the performance of an AO system when readout noise and photon noise exist at the same time is

shown in Fig. 8. It can be seen from Fig. 8 that in order to obtain a certain phase compensation effectiveness the SNR in an AO system must be large enough; if SNR is too small, the measurement error becomes larger extremely fast; when SNR is larger than a certain value (here, about 10), the improvement of the AO system performance is quite limited.

All discussions presented above do not include the corresponding change of time delay due to a change of CCD pixel number for each subaperture. This factor is included now. It is assumed that the time delay in an AO system is proportional to the CCD pixel number for each subaperture. This assumption should be quite reasonable. Further, when the CCD pixel number for each subaperture is 8×8, a time delay of 5 *ms* is chosen for an AO system. Simulation computational results of comprehensive effect under the typical conditions of larger and smaller readout noise are shown in Fig. 9. It can be seen that SNR has an apparent effect on the results and no matter the readout noise is larger or smaller a same SNR can produce a quite comparable phase compensation effectiveness. It is also shown in Fig. 9 that when the CCD pixel number for each subaperture reaches 4×4, an AO system has basically gotten a necessary measurement accuracy. Whereas because the phase correction effectiveness of an AO system depends on the time delay of the system to a great extent, it makes the benefit come from the corresponding decrease of the time delay due to decrease of the CCD pixel number for each subaperture to be larger than the loss come from the decrease of the measurement accuracy. In order to achieve the optimum working condition in an AO system, it is necessary to consider several related factors comprehensively.

4.7 Comparison of the statistics method with the formulation method

A comparison of computational results of numerical simulation by using the statistics method presented in this paper with those by using the formulation method is shown in Table 1. "No error" results in the Table are those without the detection error and noises. It is shown in Table 1 that when SNR is larger, results of the formulation method are almost same as those of the statistics method; but, when SNR is smaller, results of the formulation method are significantly different in comparison to those of the statistics method.

Table 1 Comparison of computational results of numerical simulation by using statistics method to those by using formulation method

Computational conditions: proportion of the deadspace is 0.125, CCD pixel number for each subaperture is 8×8, $\sigma_r = 2$, others are same as those in Fig. 2 besides those indicated in the Table.

Signal to noise ratio	Statistics method		Formulation method	
	E_r *(%)*	*S*	E_r *(%)*	*S*
No error	0	0.6996	0	0.6996
10000	0.2891×10^{1}	0.6993	0.2883×10^{1}	0.6993
9.806	0.1292×10^{2}	0.6948	0.1268×10^{2}	0.6981
6.804	0.3420×10^{2}	0.6884	0.4019×10^{2}	0.6954
2.673	0.4679×10^{3}	0.5869	0.7342×10^{3}	0.6367
1.667	0.1616×10^{4}	0.4025	0.2775×10^{4}	0.4981
0.816	0.9508×10^{4}	0.07869	0.1671×10^{5}	0.1418
0.447	0.4318×10^{5}	0.01575	0.6599×10^{5}	0.03230

5. CONCLUSIONS

In this paper, modeling and a numerical simulation of the effects of noise and detection error in an AO system are carried out. Numerical simulation investigations show that (i) the pixel number for each subaperture in a HS wavefront sensor must be large enough. If the number is too small the slope measurement accuracy is poor. When the number is larger than an optimum value, the loss come from the corresponding increase of the time delay due to increase of the CCD pixel number for each subaperture is significantly larger than the benefit come from the increase of the measurement accuracy. (ii) On the condition of practical deadspace proportion, the effect of deadspace is not important. (iii) SNR must be larger than a certain value. Under the condition of smaller SNR than the value, the measurement error in the wavefront sensor increases rapidly to become unacceptable. (iv) A statistics method is presented to evaluate the effects of readout noise and/or photon noise in a numerical simulation. On the condition of larger SNR, there is no significant difference between results by using the formulation method and by using the statistics method. However, as SNR gets smaller, the formulation method becomes less accurate. It is shown that a numerical simulation is very valuable in design, examination, investigation and application of a highly complex electro-optic system such as an AO system.

ACKNOWLEDGEMENT

The authors gratefully acknowledge the many helpful discussions with Prof. Genrui Cao of the Beijing Institute of Technology.

REFERENCES

1. R.K.Tyson, *Principles of Adaptive Optics*, 2nd Ed., Academic Press, Boston, 1997.
2. M.C.Roggeman, B.Welsh, *Imaging Through Turbulence*, CRC Press, Boca Raton, Florida, 1996.
3. R.V.Digumarthi, N.G.Mehta, R.M.Blankinship, "Effects of a realistic adaptive optics system on the atmospheric propagation of a high energy laser beam," *Proc. SPIE* **1221**, pp. 157-165, 1990.
4. C.A.Primmerman, T.R.Price, R.A.Humphreys, B.G.Zollars, H.T.Barclay, J.Hermann, "Atomospheric-compensation experiments in strong-scintillation conditions," *Appl. Opt.* **34**, pp. 2081-2088, 1995.
5. S.N.Gullapalli, R.Abreu, W.M.Rappoport, W.P.Zmek, R.Pringle, "Modeling of the SAAO adaptive optics system," *Proc. SPIE* **3931**, pp.285-299, 2000.
6. Hai-Xing Yan, Shu-Shan Li, De-Liang Zhang, She Chen, "Numerical simulation of an adaptive optics system with laser propagation in the atmosphere," *Appl. Opt.* **39**, pp. 3023-3031, 2000.
7. Hai-Xing Yan, Shu-Shan Li, She Chen, "Numerical simulation investigations of the dynamic control process and frequency response characteristics in an adaptive optics system," *Proc. SPIE* **4494**, a companion paper, 2001.
8. Genrui Cao, Xin Yu, "Accuracy analysis of Hartmann-Shack wavefront sensor operated with a faint object," *Opt. Eng.* **33**, pp.2331-2335, 1994.
9. T.J.Kane, B.M.Welsh, C.S.Gardner, "Wavefront detector optimization for laser guided adaptive telescopes," *Proc. SPIE* **1114**, pp.160-171, 1989.
10. J.S.Morgan, D.C.Slater, J.G.Timothy, E.B.Jenkins, "Centroid position measurements and subpixel sensitivity variations with the MAMA detector," *Appl. Opt.* **28**, pp.1178-1192, 1989.
11. Wenhan Jiang, Huagui Li, "Hartmann-Shack wavefront sensing and wavefront control algorithm," *Proc. SPIE* **1271**, pp.82-93, 1990.